ACS Chemical Neuroscience

Letter

pubs.acs.org/chemneuro

The Conformational Stability of Nonfibrillar Amyloid-β Peptide Oligomers Critically Depends on the C-Terminal Peptide Length

Eileen Socher, Heinrich Sticht,* and Anselm H. C. Horn

Bioinformatik, Institut für Biochemie, Friedrich-Alexander-Universität Erlangen-Nürnberg (FAU), Fahrstraße 17, 91054 Erlangen, Germany

Supporting Information

ABSTRACT: The amyloid-β (Aβ) peptide is one key molecule in the pathogenesis of Alzheimer's disease. We investigated the conformational stability of a nonfibrillar tetrameric Aβ structure by molecular dynamics (MD) simulations revealing that the stability of the Aβ tetramer depends critically on the C-terminal length. In contrast to the Aβ_{17-40} tetramer, which proved to be instable, the simulations demonstrate structural integrity of the Aβ_{17-42} and Aβ_{17-43} tetramers. These differences in stability can be attributed to an extension of the middle strand of a three-stranded antiparallel β sheet through residues 41−43, only present in the longer Aβ species that aggregate faster and are more neurotoxic. Additional MD simulations demonstrate that this higher stability is also present in the monomers forming the tetramer. In conclusion, our findings suggest the existence of a nonfibrillar oligomer topology that is significantly more stable for the longer Aβ species, thus offering a structural explanation for their higher neurotoxicity.

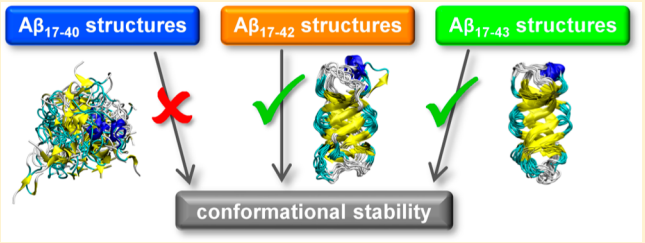

KEYWORDS: *Alzheimer's disease (AD), amyloid-β (Aβ) peptide, Abeta43, tetramer, oligomer, molecular dynamics (MD) simulations*

The amyloid-β (Aβ) peptide is one key molecule in the pathogenesis of Alzheimer's disease (AD), which is the most common neurodegenerative disorder.[1] AD is characterized by progressive dementia and the global loss of cognitive abilities. One histological hallmark is the increased presence of extracellular senile plaques, composed primarily of insoluble Aβ fibrils, which can be observed in the brain of affected patients.[2,3]

The amyloid-β peptide exists in several length variants differing at the C-terminus, for instance, as Aβ_{40}, Aβ_{42}, and Aβ_{43}. Aβ_{40} is the most abundant form.[4] The longer species Aβ_{42}, the second most abundant form, is more hydrophobic and more prone to polymerize into aggregates. Additionally, Aβ_{42} is more neurotoxic than Aβ_{40}.[5] The longer variant Aβ_{43} shows an even higher potent neurotoxicity in a dose-dependent manner as compared with Aβ_{40} and Aβ_{42}.[5] Despite its lower abundance, Aβ_{43} is deposited more frequently than Aβ_{40} in the brain of affected AD patients.[4,5]

Aβ fibrils were postulated for a long time to be the neurotoxic agents. Recent studies, however, showed a higher cytotoxicity for small Aβ oligomers than for Aβ fibrils, so that these soluble Aβ oligomers are now moving to the center of interest.[6−11] However, the structural characterization of small soluble Aβ oligomers is a challenging task due to their unstable and noncrystalline nature.[12]

In this context, computational simulations are valuable tools to study the initial steps of the Aβ aggregation process. Some of these simulations start from a disordered and flexible conformation of the individual Aβ building blocks and study the initial steps of oligomer formation.[13−18] However, these studies are computationally very expensive and it is yet not possible to sample the entire conformational space accessible to Aβ oligomers. Alternatively, MD has been used to assess the stability of Aβ oligomers. Most of these studies start from experimentally determined topologies and investigate features like oligomer length,[19,20] number of Aβ chains,[21] alternative interfaces,[22−27] effects of mutations,[28] or interaction with membranes.[29]

In addition, Aβ oligomers have been studied by biophysical methods. Solid-state NMR spectroscopy, for example, revealed that some Aβ oligomer species already contain preformed long strands as in the mature fibrils.[30,31] But there is also experimental evidence from infrared spectroscopy for the presence of antiparallel β-strands in Aβ oligomers,[11] demonstrating the existence of structural features clearly distinct from that of the fibril. In summary, all studies above demonstrate that Aβ oligomers are conformationally heterogeneous, which renders a characterization of their structural properties difficult.

One approach to tackle the problem of structural heterogeneity is to stabilize a particular defined oligomer conformation to facilitate its characterization. To achieve this goal, parts of the Aβ peptide are frequently complexed or fused with other proteins for crystallization.[32−34] In 2011, this approach resulted in the crystal structure containing the amylogenic residues 18−41 of the Aβ peptide, which were genetically engineered into the CDR3 loop region of a shark antigen receptor (IgNAR) single variable domain antibody

Published: February 4, 2014

   dx.doi.org/10.1021/cn400208r | ACS Chem. Neurosci. 2014, 5, 161−167

(PDB code: 3MOQ).[12] In this crystal structure, the Aβ-IgNAR molecules form a tight tetramer through interactions mediated by the inserted Aβ part (Figure S1, Supporting Information) and the authors suggest that this structure can be used as a potential model system for nonfibrillar oligomer formation in AD.[12]

To assess the stability of this Aβ-IgNAR crystal structure in solution, we performed a 200 ns MD simulation of this chimeric tetramer. The results showed a stable behavior of the individual subunits and the tetramer interface, although we could detect large hinge motions of the IgNAR parts with respect to each other (Figure S2, Supporting Information).

This conformational rigidity of the Aβ part in the context of the IgNAR scaffold prompted us to investigate whether Aβ exhibits a similar stability in the absence of this scaffolding protein. In the isolated Aβ part, every single chain has a triple-stranded antiparallel β sheet and neighboring sheets of two chains form a six-stranded β sheet (Figure 1).

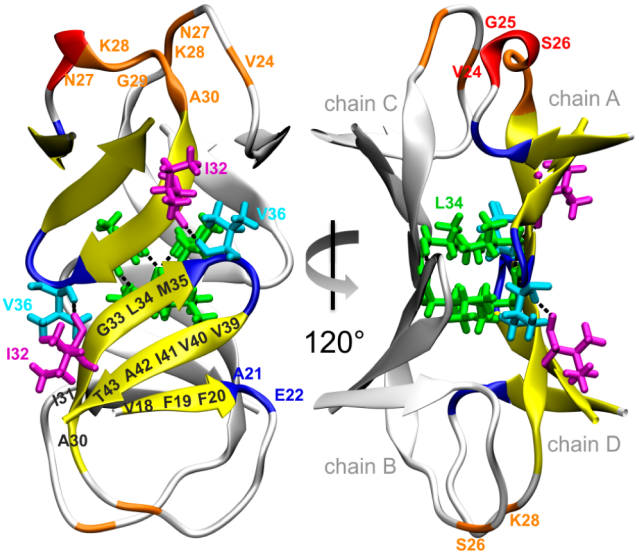

Figure 1. Starting structure of the Aβ_{17-43} tetramer. The secondary structure elements of chain A and D are colored: antiparallel β sheet in yellow, 3_{10} helix in red, and the turn in blue. The hydrophobic side chains of the Leu34 residues (green, drawn as sticks) oppose each other in the tetramer and form intermolecular backbone hydrogen bonds (black dashed line). The Ile32 (magenta) and Val36 (cyan) residues, which also form intermolecular hydrogen bonds, are shown as sticks. In contrast to Leu34, which is buried in the interface, Ile32 and Val36 expose 20−30% of their molecular surface to the solvent. For better orientation, several residues of the loop regions are colored in orange.

Since the physiologically detected Aβ species differ in the lengths of their C-termini, we performed 400 ns MD simulations for three different tetramers: Aβ_{17-40}, Aβ_{17-42}, and Aβ_{17-43}.

The respective tetrameric structures showed a clearly distinct dynamic behavior over the simulation time. The tetramers of the longer Aβ variants had much lower and more constant values of the root-mean-square deviation (RMSD) than the Aβ_{17-40} variant (Figure 2).

The magnitude of the RMSD indicates that the tetramers Aβ_{17-42} and Aβ_{17-43} are rather stable. The only larger-scale motion is the detachment of one β-strand (V18−F20) in chain A of Aβ_{17-42} after 245 ns. The strand attaches again to the

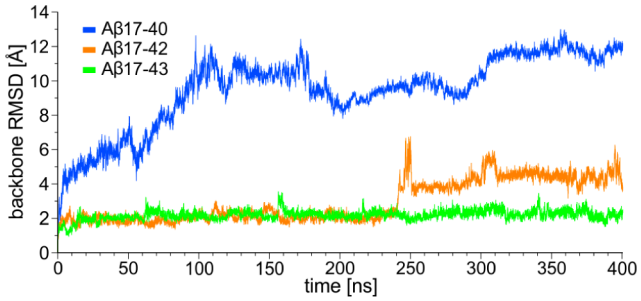

Figure 2. RMSD values over time for the tetrameric structures of Aβ_{17-40}, Aβ_{17-42}, and Aβ_{17-43}. While the tetramers Aβ_{17-42} and Aβ_{17-43} are stable, the tetramer Aβ_{17-40} is unstable over the simulation time and shows the largest deviations from the starting structure.

remaining parts of the β-sheet after 250 ns but in a slightly different orientation. These motions explain the peak at 245−250 ns in the RMSD plot (Figure 2) and the slightly increased RMSD for the remaining simulation time (see also Supplementary Movie, Supporting Information). The respective motion is a rare event, which is only observed once for one of the chains of the tetramer over the simulation time. In a 300 ns control simulation of Aβ17−42, no loss of secondary structure is observed (Figure S3, Supporting Information). In contrast to the stability detected for Aβ_{17-42} and Aβ_{17-43}, the Aβ_{17-40} tetramer is unstable over the simulation time and deviates significantly from the starting structure. These significant differences in structural stability are also confirmed by control simulations that were performed for all three tetramers (Figure S3, Supporting Information).

In the next analysis, the root-mean-square fluctuations (RMSF) were calculated for each single residue in the different chains. This analysis of the Aβ17−40 tetramer revealed high fluctuations for the terminal residues indicative of local unfolding (Figure 3A). In contrast to this, the longer Aβ variants exhibited much smaller RMSF values. In particular, the N- and C-terminal ends showed smaller fluctuations with increasing peptide length (Figure 3B and C).

To investigate and explain this in more detail, we determined the secondary structure evolution over time for the tetramers. The respective analysis (Figure 4) showed that the stability of the secondary structure elements of the tetramer increased with Aβ chain length and that most of the secondary structure elements in the Aβ_{17-40} were unstable. In particular, the β-strands at the N- and the C-terminus, which were detected in the starting structure, were not stable over 400 ns. Only the central β-strand Gly33-Met35 was retained in each chain (Figure 4A). Despite the stability of this central β-strand, the tetramer interface is significantly disrupted in Aβ_{17-40}, as evidenced by the increase of the solvent accessibility of Leu34, which constitutes the central hydrophobic residue of the interface (Figure S4, Supporting Information).

In contrast to the findings for the Aβ_{17-40} tetramer, the secondary structure elements and the tetramer interface of Aβ_{17-42} were mainly stable. Thereby, the central β-strand (Gly33-Met35) was again the most stable structure. Additionally, the C-terminally located β-strands and most of the N-terminally located β-strands were also retained. The turn Val36-Gly38, which connects the middle β-strand (Gly33-Met35) with the C-terminal β-strand (Val39-Ala42), belonged also to the stable secondary structures (Figure 4B). In the Aβ_{17-43} tetramer, all three β-strands and the two turns (Ala21-Glu22

dx.doi.org/10.1021/cn400208r | ACS Chem. Neurosci. 2014, 5, 161−167

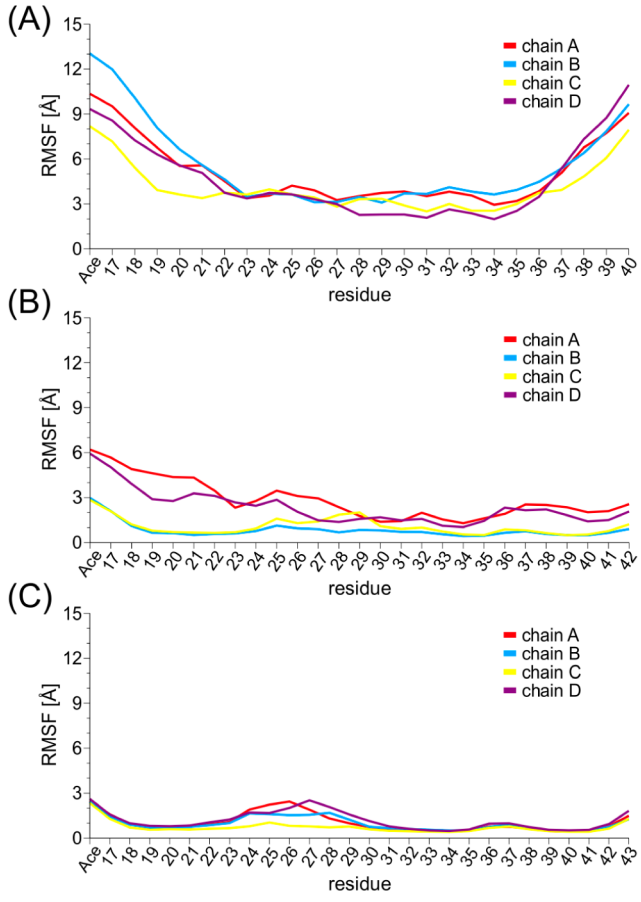

Figure 3. Fluctuation values of the backbone (RMSF) plotted as a function of the residue number for the tetrameric structures of (A) $A\beta_{17-40}$, (B) $A\beta_{17-42}$, and (C) $A\beta_{17-43}$. The longer and more hydrophobic $A\beta$ variants showed smaller fluctuations, especially at the N- and C-terminus.

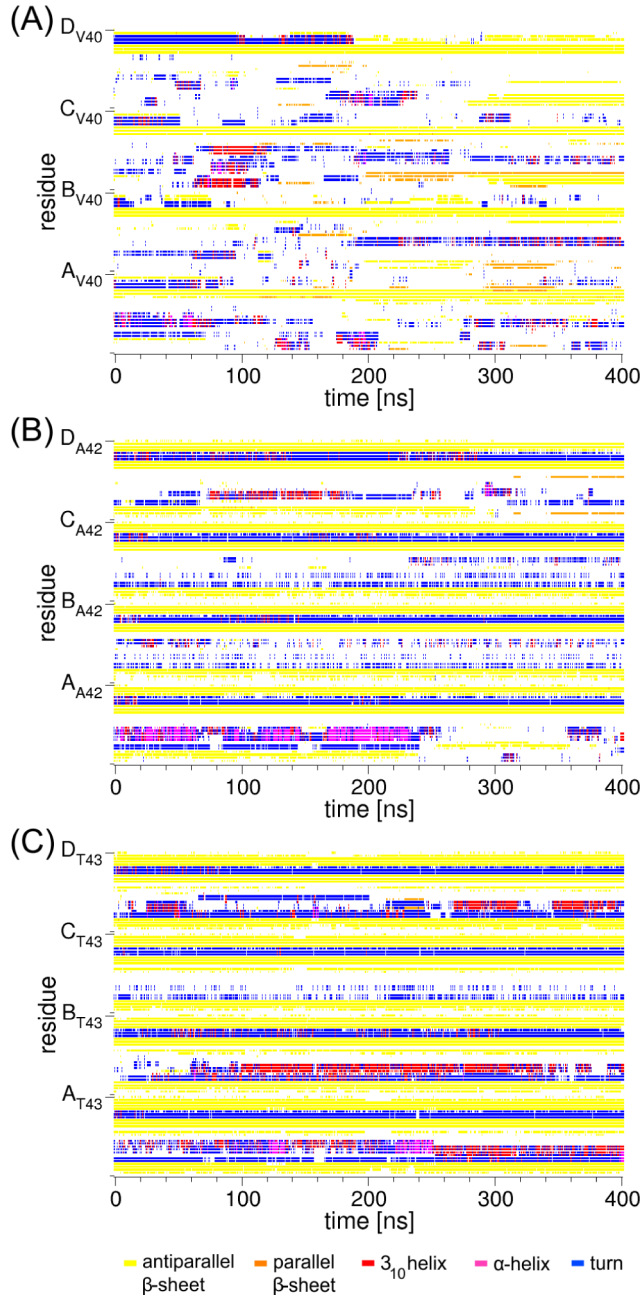

Figure 4. Secondary structure evolution of the tetramers over simulation time. The results are shown for the tetramer (A) $A\beta_{17-40}$, (B) $A\beta_{17-42}$, and (C) $A\beta_{17-43}$. Major ticks on the *y*-axis indicate the last residue of each chain, while minor ticks mark the first residues. While the secondary structure in the $A\beta_{17-40}$ tetramer lost the initial fold, the secondary structure of the starting topology could be maintained in the longer $A\beta$ variants.

and Val36-Gly38) were stabilized over the whole simulation through the C-terminal extension with residue Thr43 (Figure 4C).

We also investigated whether the present topology might be capable of pore formation, which is considered as one mechanism to confer toxicity.[35,36] Due to their tight packing, no water channels exist in the interior of the $A\beta_{17-42}$ and $A\beta_{17-43}$ structures. We did not investigate the location of water molecules for $A\beta_{17-40}$ in detail, because the entire fold is unstable, resulting in a solvation of large parts of the peptide chain.

The observed conformational stability was quantified further with an analysis of the relative β sheet content over the simulation time (Figure 5). In accordance with the high stability of the antiparallel β sheets in the $A\beta_{17-43}$ tetramer, this tetramer also had the highest amount of antiparallel β sheets, whereas the $A\beta_{17-40}$ tetramer showed the lowest relative β sheet content (Figure 5A). The decrease in β sheet content observed for $A\beta_{17-42}$ during the second half of the simulation results from the detachment of one β-strand in subunit A as described above. The increase of the β sheet content observed for $A\beta_{17-40}$ during the second half of the simulation (Figure 5A) results from the formation of alternative β sheet structures that differ from those of the starting topology. These structural rearrangements are also reflected in the number of hydrogen bonds, which is generally smaller and exhibits fluctuations for $A\beta_{17-40}$ compared to the longer tetramers (Figure 5B). This is also exemplified by the overlay of several structures collected over the simulation time (Figure 6) and the movies provided in the Supporting Information.

Interestingly, lower stability of $A\beta_{17-40}$ is also independently detected in an alternative analysis of the stabilizing residues using SRide that was performed for the initial model structures (Table S4, Supporting Information). This analysis reveals that residues Val40 and to a lesser extent also Ala42 are the key stabilizing residues in the longer $A\beta$ oligomers. Although present in $A\beta_{17-40}$, Val40 does not represent a stabilizing

dx.doi.org/10.1021/cn400208r | ACS Chem. Neurosci. 2014, 5, 161−167

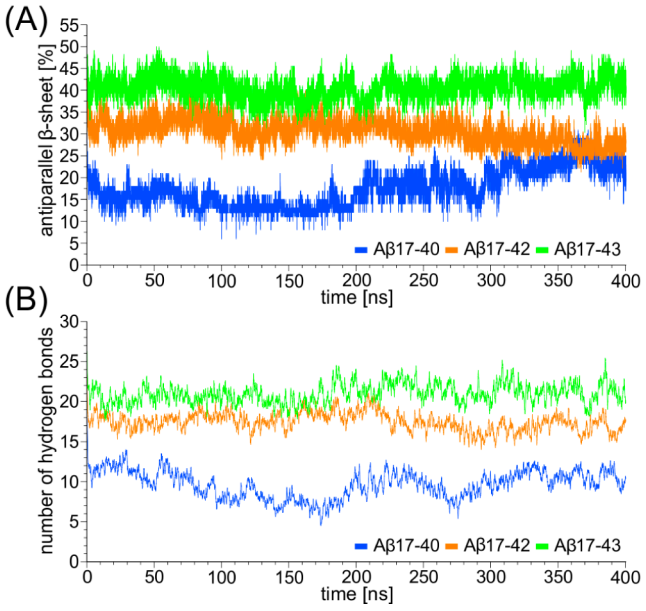

Figure 5. The β sheet content and the total number of hydrogen bonds of the tetramers versus simulation time. The longer the Aβ variant, the higher is the relative antiparallel β sheet content and the number of hydrogen bonds during simulation time.

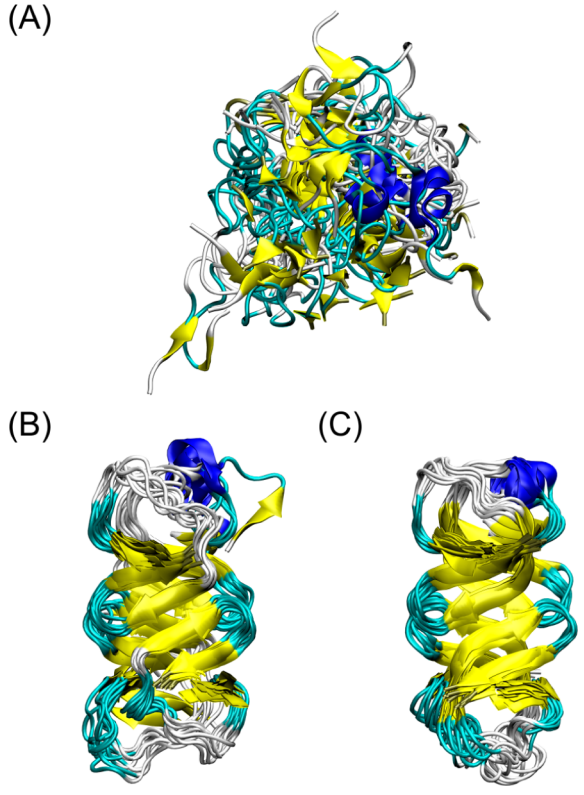

Figure 6. Overlay of every 50th nanosecond of the tetramer MD simulation of (A) Aβ_{17-40}, (B) Aβ_{17-42}, and (C) Aβ_{17-43}. The initial topology remained stable for the tetramers Aβ_{17-42} and Aβ_{17-43}, but not for the shorter Aβ_{17-40}.

residue in this shorter variant (Table S4, Supporting Information), which is in line with the large structural changes detected over the MD simulation (Figure 6). In summary, all data above demonstrate that the tetramer topology present in the Aβ-IgNAR crystal structure is stable for Aβ_{17-42} and Aβ_{17-43} but not for the shorter Aβ_{17-40}. The structural changes detected in Aβ_{17-40} include the formation of alternative β-strands, for example, between residues 18−21 of chain C and D, which might indicate an ongoing progression toward fibrillar structures. However, fibril formation itself occurs on much longer time scales[37] not yet accessible to conventional MD simulations. Therefore, an investigation of the conversion to fibrillar structures was not the aim of the present study, which instead addressed the conformational stability of a nonfibrillar oligomer topology in dependence from the C-terminal Aβ length.

Next, we investigated whether these differences in stability detected for the tetramers are also present in the monomeric building blocks. For each of the four monomers forming the tetramer independent 200 ns MD simulations were performed. This allows to assess the influence of the starting structure on the effects observed thereby avoiding an over interpretation of rarely sampled motions.

As in the tetramers, the stability of the monomers proved also to be critically affected by the length of the C-terminus. The initial topology remained stable for all Aβ_{17-43} monomers investigated, whereas none of the Aβ_{17-40} monomers remained stable. Aβ_{17-42} exhibits an intermediate stability as evidenced by the unfolding of two of the four monomers (Figure S5−S9, Table S3, Supporting Information). Although the present simulations are limited to a nanosecond time scale, these findings suggest that this topology can already be formed in the monomeric building blocks of the longer Aβ variants and subsequently become stabilized by the formation of nonfibrillar tetramers or even larger oligomers. For Aβ_{17-43}, which is the most stable variant in this study, these results also support the suggestion that Aβ_{43} could initiate the formation of oligomers and amyloid plaques and thereby be crucial for AD pathogenesis.[38]

Thus, our study provides the first computational investigation of this novel Aβ tetramer topology. One limitation of the template crystal structure,[12] which represents the only high-resolution structure of a nonfibrillar oligomer to date, is the absence of the N-terminus. We refrained from modeling the N-terminus for the following reasons: The N-terminus exerts multiple different functions as a phosphorylation site or metal ion binding site, and it exhibits a structural role in mature fibrils.[39−42] Thus, the N-terminus can adopt multiple distinct conformations depending on the oligomerization state or environmental conditions, for example, the presence of metal ions. Therefore, it appears extremely difficult to model the correct state of the N-terminus in the absence of further experimental knowledge.

In addition, the present MD simulations indicate that the Aβ_{17-42} and Aβ_{17-43} oligomers are stable in the absence of the N-terminus, indicating that the latter is not required for maintaining the oligomer topology. Nevertheless, we are aware that the presence of the N-terminus might affect the overall stability of the tetramer. For this reason, the emphasis of the present work is not on the overall tetramer stability but rather on the relative stability of tetramers of differing in their C-terminal length. Therefore, we feel that the conclusions drawn from the present study remain also relevant for the full-length Aβ-peptides.

The conducted MD simulations revealed that the investigated tetramers of the longer Aβ variants were significantly more stable than the shorter Aβ_{17-40} tetramer. Further, the structures of the longer variants were very similar to the starting

dx.doi.org/10.1021/cn400208r | ACS Chem. Neurosci. 2014, 5, 161−167

structure throughout the 400 ns long simulations, as reflected in low average RMSD values. As opposed to this, the tetramer $A\beta_{17-40}$ showed very high RMSD and RMSF values and no stable secondary structure elements, indicating a loss of the initial fold. The elongation of the C-terminus by the residues 41 and 42 or the residues 41−43 increases the stability of the investigated structures, because these additional residues elongate the middle strand of a three-stranded antiparallel β sheet (Figure 1). For that reason, the length of the C-terminus of the Aβ fragment seems to be critical for the stability of this topology. This property is particularly remarkable, since $A\beta_{40}$ and $A\beta_{42}$ form quite similar U-shaped fibrillar topologies consisting of two stacks of parallel in-register β sheets.[43,44]

Cross-β topologies have recently also been reported for toxic fibrillar oligomers that contain 19 ± 4 Aβ-chains.[45] However, toxicity is also observed for much smaller oligomers like dimers and tetramers.[6,37,46] These small oligomers exhibit a large conformational variability rendering an investigation of alternative nonfibrillar conformations highly relevant. In addition, an analysis of fibrillar topologies frequently offered only a limited explanation for the differences in aggregation tendency and neurotoxicity of different Aβ species.

In this context, the present study suggests that the formation of nonfibrillar oligomers might be much more dependent on the length of the Aβ C-terminus. The tetramer investigated here is entirely instable for $A\beta_{17-40}$, indicating that this topology can exclusively be established for the longer $A\beta_{17-42}$ and $A\beta_{17-43}$, thus representing an Aβ variant-specific conformation. Since the longer Aβ variants are also the more neurotoxic agents,[5] the present topology may help to explain some of the neurotoxic Aβ effects. In addition, the existence of a nonfibrillar oligomeric fold that is particularly stable in the longer and more neurotoxic Aβ species might also be helpful for antibody design or rational drug design aiming at the prevention of oligomer formation.

METHODS

Preparation of Starting Structures. The crystal structure of the Aβ-IgNAR chimeric tetramer was used as a template for the preparation of the starting structures (PDB code: 3MOQ;[12] resolution: 2.05 Å). This construct contains residues 18−41 of Aβ that are inserted between residues 87 and 112 of the antibody scaffold. For generating the starting structure of the tetrameric Aβ-IgNAR, the C-terminal alanine residues were capped by *N*-methylamine (NME) in each chain. For generating the tetrameric $A\beta_{17-43}$ structure from the crystal structure, residues 1−86 and 114−126 that belong to the antibody moiety were deleted. The tyrosine at position 87 of the antibody was mutated to leucine to generate Aβ residue Leu17, which is part of the central hydrophobic core and important for β sheet formation in fibril conformations.[47] Because the N-terminus of the present model is not the first residue of the naturally occurring Aβ, Leu17 was acetylated using SYBYL 7.3[48] to avoid artifacts by a nonphysiologically charged end group. Subsequently, residues 112 and 113 of the antibody were changed to alanine and threonine, respectively, resulting in the $A\beta_{17-43}$ structure. To obtain the $A\beta_{17-40}$ and $A\beta_{17-42}$ tetramers, the last one or last three residues at the C-terminus of the single chains of the $A\beta_{17-43}$ tetramer were deleted. All these C-termini were kept ionic. For the generation of the monomeric structures, the corresponding tetramer was used and the nonrequired chains were removed. For an easier comparison with previous studies of the amyloid-β peptide, the numbering scheme of the residues corresponds to that used for the full length Aβ: $LVFF_{20}AEDVGS-NKGA_{30}IIGLMVGGVV_{40}IAT$.

Stabilizing residues in the tetrameric starting structures of $A\beta_{17-40}$, $A\beta_{17-42}$, and $A\beta_{17-43}$ were identified with SRide[49] (http://sride.enzim.hu/) using standard settings.

Molecular Dynamics Simulations. Molecular dynamics simulations were performed using version 11 of the AMBER Molecular Dynamics software package[50] (ambermd.org) and the ff99SB force field.[51,52] With the AMBER tool LEaP, all systems were electrically neutralized with Na^+ or Cl^- ions and solvated with TIP3P[53] water molecules (Tables S1 and S2, Supporting Information).

At first, a minimization was carried out in three subsequent steps to optimize the geometry of the starting structures. In the first step of the minimization, the water molecules were minimized while all remaining atoms were restrained with a constant force of 10 kcal·mol^{-1}·Å^{-2} to the initial positions. In the second step, additional relaxation of the sodium ions and the hydrogen atoms of the protein were allowed, while the remaining protein was restrained with 10 kcal·mol^{-1}·Å^{-2}. In the last step, no restrains were used, so that the whole protein, the ions, and the water molecules were minimized. All three minimization parts started with 2500 steps using the steepest descent algorithm, followed by 2500 steps of a conjugate gradient minimization.

After the minimization, the systems were equilibrated in two successive steps. In the first step, the temperature was raised from 10 to 310 K within 0.1 ns and the protein was restrained with a constant force of 5 kcal·mol^{-1}·Å^{-2}. In the second step (0.4 ns length), only the Cα atoms of the protein were restrained with a constant force of 5 kcal·mol^{-1}·Å^{-2}. In both equilibration steps, the time step was 2 fs.

In the following, 100−400 ns long production phases were performed at 310 K, without any restraints and with a time step of 2 fs. For bonds involving hydrogen, the SHAKE algorithm was applied in the equilibration and production phase. Furthermore, the constant pressure periodic boundary conditions were used with an average pressure of 1 bar and isotropic position scaling. A Berendsen thermostat was used to maintain the temperature of the system at 310 K. The AMBER tool ptraj or the programs VMD[54] and DSSP (Define Secondary Structure of Proteins)[55] were used for structure analysis. All molecular illustrations were made with VMD.

ASSOCIATED CONTENT

Supporting Information

Additional as described in text. This material is available free of charge via the Internet at http://pubs.acs.org.

AUTHOR INFORMATION

Corresponding Author

*E-mail: heinrich.sticht@fau.de.

Author Contributions

E.S., H.S., and A.H.C.H. designed the study. E.S. performed the simulations and analyses. E.S, H.S., and A.H.C.H. wrote the manuscript. H.S. and A.H.C.H. supervised the project.

Notes

The authors declare no competing financial interest.

ACKNOWLEDGMENTS

We thank the High Performance Computing Group of the Regionales Rechenzentrum Erlangen for AMBER executables optimized for parallel execution. We would also like to thank Victoria Jackiw for helpful comments on the manuscript.

ABBREVIATIONS

Aβ, amyloid-β peptide; MD, molecular dynamics; AD, Alzheimer's disease; RMSD, root-mean-square deviation; RMSF, root-mean-square fluctuations

REFERENCES

(1) Bertram, L., Lill, C. M., and Tanzi, R. E. (2010) The Genetics of Alzheimer Disease: Back to the Future. *Neuron 68*, 270−281.

(2) Finder, V. H., and Glockshuber, R. (2007) Amyloid-β Aggregation. *Neurodegener. Dis. 4*, 13−27.

(3) Ahmed, M., Davis, J., Aucoin, D., Sato, T., Ahuja, S., Aimoto, S., Elliott, J. I., van Nostrand, W. E., and Smith, S. O. (2010) Structural conversion of neurotoxic amyloid-β(1−42) oligomers to fibrils. *Nat. Struct. Mol. Biol. 17*, 561−567.
(4) Welander, H., Frånberg, J., Graff, C., Sundström, E., Winblad, B., and Tjernberg, L. O. (2009) Aβ43 is more frequent than Aβ40 in amyloid plaque cores from Alzheimer disease brains. *J. Neurochem. 110*, 697−706.
(5) Saito, T., Suemoto, T., Brouwers, N., Sleegers, K., Funamoto, S., Mihira, N., Matsuba, Y., Yamada, K., Nilsson, P., Takano, J., Nishimura, M., Iwata, N., Broeckhoven, C., Van Ihara, Y., and Saido, T. C. (2011) Potent amyloidogenicity and pathogenicity of Aβ43. *Nat. Neurosci. 14*, 1023−1032.
(6) Dahlgren, K. N., Manelli, A. M., Stine, W. B., Jr, Baker, L. K., Krafft, G. A., and LaDu, M. J. (2002) Oligomeric and fibrillar species of amyloid-beta peptides differentially affect neuronal viability. *J. Biol. Chem. 277*, 32046−32053.
(7) Cleary, J. P., Walsh, D. M., Hofmeister, J. J., Shankar, G. M., Kuskowski, M. A., Selkoe, D. J., and Ashe, K. H. (2005) Natural oligomers of the amyloid-beta protein specifically disrupt cognitive function. *Nat. Neurosci. 8*, 79−84.
(8) McLean, C. A., Cherny, R. A., Fraser, F. W., Fuller, S. J., Smith, M. J., Beyreuther, K., Bush, A. I., and Masters, C. L. (1999) Soluble Pool of Aβ Amyloid as a Determinant of Severity of Neurodegeneration in Alzheimer's Disease. *Ann. Neurol. 46*, 860−866.
(9) Lesne, S., Koh, M. T., Kotilinek, L., Kayed, R., Glabe, C. G., Yang, A., Gallagher, M., and Ashe, K. H. (2006) A specific amyloid-beta protein assembly in the brain impairs memory. *Nature 440*, 352−357.
(10) Walsh, D. M., and Selkoe, D. J. (2004) Oligomers on the brain: the emerging role of soluble protein aggregates in neurodegeneration. *Protein Pept. Lett. 11*, 213−228.
(11) Fändrich, M. (2012) Oligomeric Intermediates in Amyloid Formation: Structure Determination and Mechanisms of Toxicity. *J. Mol. Biol. 421*, 427−440.
(12) Streltsov, V. A., Varghese, J. N., Masters, C. L., and Nuttall, S. D. (2011) Crystal Structure of the Amyloid-β p3 Fragment Provides a Model for Oligomer Formation in Alzheimer's Disease. *J. Neurosci. 31*, 1419−1426.
(13) Wei, G., Jewett, A. I., and Shea, J.-E. (2010) Structural diversity of dimers of the Alzheimer amyloid-β(25−35) peptide and polymorphism of the resulting fibrils. *Phys. Chem. Chem. Phys. 12*, 3622−3629.
(14) Anand, P., Nandel, F. S., and Hansmann, U. H. E. (2008) The Alzheimer β-amyloid (Aβ1−39) dimer in an implicit solvent. *J. Chem. Phys. 129*, 195102.
(15) Côté, S., Laghaei, R., Derreumaux, P., and Mousseau, N. (2012) Distinct Dimerization for Various Alloforms of the Amyloid-Beta Protein: Aβ1−40, Aβ1−42, and Aβ1−40(D23N). *J. Phys. Chem. B 116*, 4043−4055.
(16) Kim, S., Takeda, T., and Klimov, D. K. (2010) Mapping Conformational Ensembles of Aβ Oligomers in Molecular Dynamics Simulations. *Biophys. J. 99*, 1949−1958.
(17) Gnanakaran, S., Nussinov, R., and García, A. E. (2006) Atomic-Level Description of Amyloid β-Dimer Formation. *J. Am. Chem. Soc. 128*, 2158−2159.
(18) Shea, J.-E., and Urbanc, B. (2012) Insights into Aβ aggregation: a molecular dynamics perspective. *Curr. Top. Med. Chem. (Sharjah, United Arab Emirates) 12*, 2596−2610.
(19) Huet, A., and Derreumaux, P. (2006) Impact of the Mutation A21G (Flemish Variant) on Alzheimer's β-Amyloid Dimers by Molecular Dynamics Simulations. *Biophys. J. 91*, 3829−3840.
(20) Viet, M. H., Nguyen, P. H., Ngo, S. T., Li, M. S., and Derreumaux, P. (2013) Effect of the Tottori Familial Disease Mutation (D7N) on the Monomers and Dimers of Aβ40 and Aβ42. *ACS Chem. Neurosci. 4*, 1446−1457.
(21) Horn, A. H. C., and Sticht, H. (2010) Amyloid-β42 Oligomer Structures from Fibrils: A Systematic Molecular Dynamics Study. *J. Phys. Chem. B 114*, 2219−2226.
(22) Zheng, J., Jang, H., Ma, B., Tsai, C.-J., and Nussinov, R. (2007) Modeling the Alzheimer Aβ17−42 Fibril Architecture: Tight Intermolecular Sheet-Sheet Association and Intramolecular Hydrated Cavities. *Biophys. J. 93*, 3046−3057.
(23) Wu, C., Bowers, M. T., and Shea, J.-E. (2010) Molecular Structures of Quiescently Grown and Brain-Derived Polymorphic Fibrils of the Alzheimer Amyloid Aβ9−40 Peptide: A Comparison to Agitated Fibrils. *PLoS Comput. Biol 6*, e1000693.
(24) Miller, Y., Ma, B., and Nussinov, R. (2011) The Unique Alzheimer's β-Amyloid Triangular Fibril Has a Cavity along the Fibril Axis under Physiological Conditions. *J. Am. Chem. Soc. 133*, 2742−2748.
(25) Zheng, J., Yu, X., Wang, J., Yang, J.-C., and Wang, Q. (2010) Molecular Modeling of Two Distinct Triangular Oligomers in Amyloid β-protein. *J. Phys. Chem. B 114*, 463−470.
(26) Berhanu, W. M., and Hansmann, U. H. E. (2012) Structure and Dynamics of Amyloid-β Segmental Polymorphisms. *PLoS One 7*, e41479.
(27) Kahler, A., Sticht, H., and Horn, A. H. C. (2013) Conformational Stability of Fibrillar Amyloid-Beta Oligomers via Protofilament Pair Formation - A Systematic Computational Study. *PLoS One 8*, e70521.
(28) Kassler, K., Horn, A. H. C., and Sticht, H. (2010) Effect of pathogenic mutations on the structure and dynamics of Alzheimer's Aβ42-amyloid oligomers. *J. Mol. Model. 16*, 1011−1020.
(29) Jang, H., Connelly, L., Arce, F. T., Ramachandran, S., Kagan, B. L., Lal, R., and Nussinov, R. (2013) Mechanisms for the Insertion of Toxic, Fibril-like β-Amyloid Oligomers into the Membrane. *J. Chem. Theory Comput. 9*, 822−833.
(30) Bertini, I., Gallo, G., Korsak, M., Luchinat, C., Mao, J., and Ravera, E. (2013) Formation Kinetics and Structural Features of Beta-Amyloid Aggregates by Sedimented Solute NMR. *ChemBioChem 14*, 1891−1897.
(31) Fawzi, N. L., Ying, J., Ghirlando, R., Torchia, D. A., and Clore, G. M. (2011) Atomic-resolution dynamics on the surface of amyloid-β protofibrils probed by solution NMR. *Nature 480*, 268−272.
(32) Shen, Y., Joachimiak, A., Rosner, M. R., and Tang, W.-J. (2006) Structures of human insulin-degrading enzyme reveal a new substrate recognition mechanism. *Nature 443*, 870−874.
(33) Gardberg, A. S., Dice, L. T., Ou, S., Rich, R. L., Helmbrecht, E., Ko, J., Wetzel, R., Myszka, D. G., Patterson, P. H., and Dealwis, C. (2007) Molecular basis for passive immunotherapy of Alzheimer's disease. *Proc. Natl. Acad. Sci. U.S.A. 104*, 15659−15664.
(34) Takano, K., Endo, S., Mukaiyama, A., Chon, H., Matsumura, H., Koga, Y., and Kanaya, S. (2006) Structure of amyloid β fragments in aqueous environments. *FEBS J. 273*, 150−158.
(35) Jang, H., Arce, F. T., Ramachandran, S., Capone, R., Azimova, R., Kagan, B. L., Nussinov, R., and Lal, R. (2010) Truncated β-amyloid peptide channels provide an alternative mechanism for Alzheimer's Disease and Down syndrome. *Proc. Natl. Acad. Sci. U.S.A. 107*, 6538−6543.
(36) Berhanu, W. M., Yasar, F., and Hansmann, U. H. E. (2013) In Silico Cross Seeding of Aβ and Amylin Fibril-like Oligomers. *ACS Chem. Neurosci. 4*, 1488−1500.
(37) Ono, K., Condron, M. M., and Teplow, D. B. (2009) Structure-neurotoxicity relationships of amyloid β-protein oligomers. *Proc. Natl. Acad. Sci. U.S.A. 106*, 14745−14750.
(38) Sandebring, A., Welander, H., Winblad, B., Graff, C., and Tjernberg, L. O. (2013) The pathogenic abeta43 is enriched in familial and sporadic Alzheimer disease. *PLoS One 8*, e55847.
(39) Kumar, S., and Walter, J. (2011) Phosphorylation of amyloid beta (Aβ) peptides - A trigger for formation of toxic aggregates in Alzheimer's disease. *Aging 3*, 803−812.
(40) Drew, S. C., Masters, C. L., and Barnham, K. J. (2010) Alzheimer's Aβ peptides with disease-associated N-terminal modifications: influence of isomerisation, truncation and mutation on Cu2+coordination. *PLoS One 5*, e15875.

(41) Yang, D. S., McLaurin, J., Qin, K., Westaway, D., and Fraser, P. E. (2000) Examining the zinc binding site of the amyloid-β peptide. *Eur. J. Biochem. 267*, 6692−6698.
(42) Lu, J.-X., Qiang, W., Yau, W.-M., Schwieters, C. D., Meredith, S. C., and Tycko, R. (2013) Molecular Structure of β-Amyloid Fibrils in Alzheimer's Disease Brain Tissue. *Cell 154*, 1257−1268.
(43) Lührs, T., Ritter, C., Adrian, M., Riek-Loher, D., Bohrmann, B., Döbeli, H., Schubert, D., and Riek, R. (2005) 3D structure of Alzheimer's amyloid-β(1−42) fibrils. *Proc. Natl. Acad. Sci. U.S.A. 102*, 17342−17347.
(44) Petkova, A. T., Ishii, Y., Balbach, J. J., Antzutkin, O. N., Leapman, R. D., Delaglio, F., and Tycko, R. (2002) A structural model for Alzheimer's beta -amyloid fibrils based on experimental constraints from solid state NMR. *Proc. Natl. Acad. Sci. U.S.A. 99*, 16742−16747.
(45) Stroud, J. C., Liu, C., Teng, P. K., and Eisenberg, D. (2012) Toxic fibrillar oligomers of amyloid-β have cross-β structure. *Proc. Natl. Acad. Sci. U.S.A. 109*, 7717−7722.
(46) Shankar, G. M., Li, S., Mehta, T. H., Garcia-Munoz, A., Shepardson, N. E., Smith, I., Brett, F. M., Farrell, M. A., Rowan, M. J., Lemere, C. A., Regan, C. M., Walsh, D. M., Sabatini, B. L., and Selkoe, D. J. (2008) Amyloid-β protein dimers isolated directly from Alzheimer's brains impair synaptic plasticity and memory. *Nat. Med. 14*, 837−842.
(47) Melquiond, A., Dong, X., Mousseau, N., and Derreumaux, P. (2008) Role of the Region 23−28 in Aβ Fibril Formation: Insights from Simulations of the Monomers and Dimers of Alzheimer's Peptides Aβ40 and Aβ42. *Curr. Alzheimer Res. 5*, 244−250.
(48) *SYBYL 7.3*, Tripos International, 1699 South Hanley Rd., St. Louis, Missouri, 63144, USA.
(49) Magyar, C., Gromiha, M. M., Pujadas, G., Tusnády, G. E., and Simon, I. (2005) SRide: a server for identifying stabilizing residues in proteins. *Nucleic Acids Res. 33*, W303−W305.
(50) Case, D. A., Darden, T. A., Cheatham, III, T. E., Simmerling, C. L., Wang, J., Duke, R. E., Luo, R., Walker, R. C., Zhang, W., Merz, K. M., Roberts, B., Wang, B., Hayik, S., Roitberg, A., Seabra, G., Kolossváry, I., Wong, K. F., Paesani, F., Vanicek, J., Liu, J., Wu, X., Brozell, S. R., Steinbrecher, T., Gohlke, H., Cai, Q., Ye, X., Hsieh, M.-J., Cui, G., Roe, D. R., Mathews, D. H., Seetin, M. G., Sagui, C., Babin, V., Luchko, T., Gusarov, S., Kovalenko, A., and Kollman, P. A. (2010) *AMBER 11*, University of California, San Francisco.
(51) Hornak, V., Abel, R., Okur, A., Strockbine, B., Roitberg, A., and Simmerling, C. (2006) Comparison of Multiple Amber Force Fields and Development of Improved Protein Backbone Parameters. *Proteins 65*, 712−725.
(52) Wang, J., Cieplak, P., and Kollman, P. A. (2000) How Well Does a Restrained Electrostatic Potential (RESP) Model Perform in Calculating Conformational Energies of Organic and Biological Molecules? *J. Comput. Chem. 21*, 1049−1074.
(53) Jorgensen, W. L., Chandrasekhar, J., Madura, J. D., Impey, R. W., and Klein, M. L. (1983) Comparison of simple potential functions for simulating liquid water. *J. Chem. Phys. 79*, 926.
(54) Humphrey, W., Dalke, A., and Schulten, K. (1996) VMD: Visual Molecular Dynamics. *J. Mol. Graphics 14*, 33−38.
(55) Kabsch, W., and Sander, C. (1983) Dictionary of Protein Secondary Structure: Pattern Recognition of Hydrogen-Bonded and Geometrical Features. *Biopolymers 22*, 2577−2637.